Extreme waveform compression with a nonlinear temporal focusing mirror

Nicolas Berti, Stéphane Coen, Miro Erkintalo, Julien Fatome

▶ **To cite this version:**

Nicolas Berti, Stéphane Coen, Miro Erkintalo, Julien Fatome. Extreme waveform compression with a nonlinear temporal focusing mirror. Nature Photonics, 2022, 16 (12), pp.822-827. 10.1038/s41566-022-01072-1 . hal-04413110

HAL Id: hal-04413110
https://hal.science/hal-04413110

Submitted on 23 Jan 2024

HAL is a multi-disciplinary open access archive for the deposit and dissemination of scientific research documents, whether they are published or not. The documents may come from teaching and research institutions in France or abroad, or from public or private research centers.

L'archive ouverte pluridisciplinaire **HAL**, est destinée au dépôt et à la diffusion de documents scientifiques de niveau recherche, publiés ou non, émanant des établissements d'enseignement et de recherche français ou étrangers, des laboratoires publics ou privés.

Extreme waveform compression with a nonlinear temporal focusing mirror

Nicolas Berti,[1] Stéphane Coen,[2,3] Miro Erkintalo[2,3] and Julien Fatome[1,2,3*]

[1]*Laboratoire Interdisciplinaire Carnot de Bourgogne, UMR 6303 CNRS Université Bourgogne Franche-Comté, Dijon, France*
[2]*Department of Physics, The University of Auckland, Private Bag 92019, Auckland 1142, New Zealand*
[3]*The Dodd-Walls Centre for Photonic and Quantum Technologies, New Zealand*
*Corresponding author: Julien.Fatome@u-bourgogne.fr

Abstract. Dealing with the increase of digital optical data transmission rates requires innovative approaches for stretching or compressing optical waveforms beyond the bandwidth limitations inherent to conventional electro-optical systems. To this aim, photonic platforms exploiting ultrafast nonlinear phenomena have been successfully applied to the temporal stretching of optical waveforms. However, the inverse process, the temporal compression of arbitrary light-waves, has remained largely unexploited so far. Here, we present an experimental demonstration of extreme temporal compression of in-fibre waveforms, including non-trivial on-demand time reversal. The method is based on counter-propagating degenerate four-photon interaction in birefringent optical fibres. We demonstrate the performance of this system by generating ultrafast replica of data packets with record temporal compression factors ranging from 4,350 to 13,000. This approach is scalable and offers great promise for ultrafast arbitrary optical waveform generation and related applications.

1. Introduction

The ability to control and modify the timescale of optical data and waveforms beyond the bandwidth limitations of conventional electro-optic technology is an essential functionality targeted in many applications, including microscopy, spectroscopy, sensing or ultrafast optical communications[1-8]. In this context, most studies have predominantly focussed on the problem of temporal *stretching*, i.e., magnification of the timescale of short temporal events such that they can be detected using traditional narrow bandwidth electronics. In particular, so-called "temporal microscopes" based on the time-lens concept[6-12], which relies on the space-time duality of electromagnetic waves, have opened up new frontiers in photonics, unveiling transient phenomena and nonlinear dynamics previously inaccessible. These time-stretching devices have led to seminal results ranging from single-shot spectroscopy[13] to real-time measurements of rogue waves[14-17], soliton explosion[18], or self-organization in mode-locked lasers[19-20]. Further advances based on anamorphic time-lens transformations have also enabled the manipulation of the time-bandwidth product of analog signals and real-time optimization of digitization[21-22].

Despite the remarkable impact of temporal *stretching* in photonics, the converse operation — the temporal *compression* of arbitrary light-waves — still remains a challenging and under-exploited functionality[23-29]. This is surprising, as such photonic temporal compressors could be advantageous in numerous contexts, for example to generate ultrafast optical signals[30-31], to increase the granularity of optical networks[32-33], for coherent control in spectroscopy or quantum processes[34-35] or to overcome bottlenecks in real-time imaging and sensing instruments[36-38]. Many early attempts at temporal waveform compression have consisted in manipulating the signal repetition-rate with time-interleaving methods, using optical buffers and delay lines[23-26]. These techniques have also been combined with spectro-temporal manipulations, and they have achieved successful compression of four-bit packets from 10 to 40 Gbit/s[27-28]. Fundamentally, however, most of these methods leave the duration of individual pulses unchanged, and the input pulse duration must be short enough to accommodate the output repetition-rate. Moreover, these methods cannot be applied to the temporal compression of arbitrary-shaped optical waveforms. More recently, the time-lens concept has been turned backward to realize a temporal telescope[28-29]. Exploiting four-wave mixing (FWM) of co-propagating pulses in optical waveguides, such systems have achieved a temporal compression factor of 27 with ns-waveforms and 10-Gbit/s data packets[29]. However, the focusing capabilities of time lenses are fundamentally restricted by practical limitations, including aberrations stemming from high-order chromatic dispersion[7,29].

In this context, it is fascinating to note that an altogether different approach was theoretically put forward in 1996 by A. Starodumov, who suggested that FWM interactions occurring during the ultrafast collisions between counter-propagating light-waves in optical fibres could be leveraged for the temporal compression of periodic pulse trains[39]. In Starodumov's proposed scheme, temporal focusing is obtained by reflecting the input waveform off a moving mirror induced by the combined effects of optical nonlinearity and fibre birefringence. However, despite offering potential solutions to deficiencies that impact existing methods, no experimental demonstration has been reported to date – to the best of our knowledge. In this contribution, we present the first experimental demonstration of Starodumov's compression scheme, and report extreme temporal compression of optical waveforms by factors ranging from 4,350 to 13,000 – results that correspond to several orders of magnitude improvement with respect to current state-of-the-art[23-29]. In addition to confirming Starodumov's original predictions of periodic pulse train compression[39], we generalize the concept to achieve on-demand time-reversal capabilities and compression of arbitrary waveforms. Our experimental results are in good agreement with theory and simulations, establishing a new tool for the manipulation of ultrafast optical data and waveforms.

2. Principle of operation

Our temporal compressor scheme corresponds to a fully-degenerate variant of Starodumov' original concept[39] and leverages the nonlinear interaction between counter-propagating light-waves in a birefringent optical waveguide[40-43] [see Fig. 1a and Supplementary movie 1]. From one end of the waveguide, a low-bandwidth optical signal carrying the input waveform to be compressed (red) is injected with a polarization state aligned at 45° with respect to the *slow* and *fast* birefringent axes (step 1 in Fig. 1a). In this way, the two polarization axes of the fibre are equally excited, which maximizes the efficiency of the underlying FWM process [see Methods for more details]. Note that, for simplicity, the illustration in Fig. 1a shows a waveform consisting of discrete bits, but the process extends to arbitrary analog waveforms [see Supplementary movie 2]. From the opposite end of the waveguide,

a single short readout pulse (green), is then injected along the *slow* polarization axis. When the readout pulse overlaps with a part of the waveform coming from the opposite direction (step 2), nonlinear FWM occurs at the collision point [see bottom inset in Fig. 1a], which leads to the generation of a new signal (blue), co-propagating and orthogonally polarized to the readout pulse. Because of birefringence, that new waveform propagates at a different group-velocity and progressively separates from the read-out pulse (step 3). The process repeats as the readout pulse encounters subsequent parts of the input waveform (steps 4-5). Overall, the generated signal is an ultrafast replica of the low-bandwidth incident light-wave. In essence, the two counter-propagating waves form an ultrafast nonlinear grating which acts as a moving mirror, reflecting and compressing the incident waveform [see inset on top of Fig. 1a]. Alternatively, the process can be interpreted as a scattering of the readout pulse by the counter-propagating waveform. Note that launching the readout pulse on the *fast* birefringent axis of the waveguide instead of the *slow* one results in a non-trivial time-reversed compressed replica [see Supplementary movie 3]. Regardless of which axis the readout pulse is launched into, the temporal compression factor M is given by the ratio between the collision speed and the rate at which the generated signal walks away from the readout pulse, i.e.,

$$M = \frac{2n_g}{|\Delta n_g|}, \qquad (1)$$

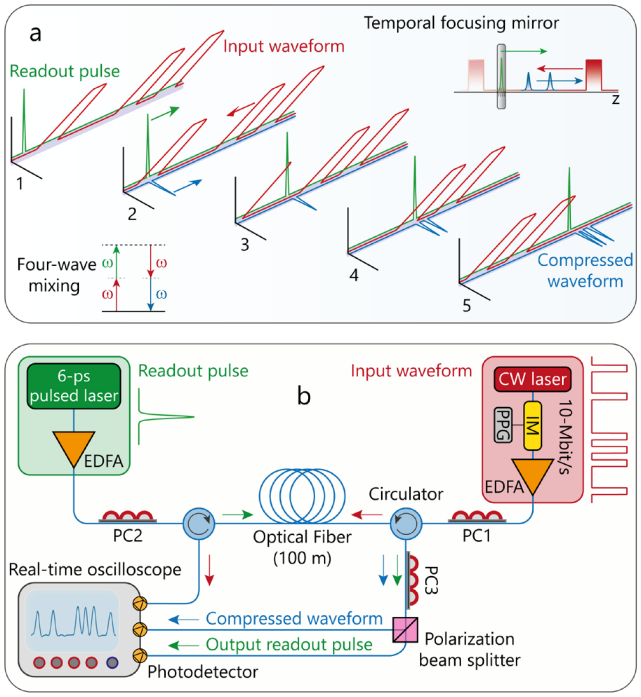

Figure 1 | Temporal compression system. (a) illustrates the principle of operation. A low-bandwidth input waveform (red) is launched into a birefringent waveguide with a linear polarization state aligned at 45° with respect to the birefringence axes (step 1). A short readout pulse (green) travels in the opposite direction, polarized along one specific axis. When both signals overlap, FWM generates a new light-wave (blue) co-propagating with and orthogonally polarized to the readout pulse (step 2). Birefringence temporally separates this generated signal from the readout pulse (step 3). The process repeats for subsequent parts of the input waveform (step 4). At the output of the waveguide, the generated signal is an ultrafast replica of the initial waveform (step 5). The top inset depicts the concept of temporal focusing mirror, whilst the bottom inset displays the underlying fully-degenerate FWM interaction. **(b)** Experimental setup. EDFA: Erbium-doped fibre amplifier, PC: Polarization controller, CW: Continuous wave, PPG: Pulse pattern generator, IM: Intensity modulator.

where n_g and Δn_g are respectively the group index seen by the readout pulse and the group index difference between the two principal axes of the waveguide. Standard birefringent optical fibres can readily provide compression factors from 10^3 to 10^4, enabling the generation of optical waveforms with several THz of bandwidth from initial signals synthetized with off-the-shelf apparatus at conventional RF frequencies (MHz or GHz). In terms of length, the waveguide must simply be longer than half the spatial extent of the input low-bandwidth waveform. Finally, we note that the shortest temporal feature that can be generated is set by the readout pulse duration τ; the input waveform is effectively convolved with a temporal window of duration $M\tau$.

3. Results

Experimental implementation

The scheme presented above was experimentally implemented as depicted in Fig. 1b [see Methods for more details]. For our demonstration, we use a 103-m-long birefringent (polarization maintaining) optical fibre, with $\Delta n_g = 6.67 \times 10^{-4}$ (corresponding to a walk-off rate of 2.22 ps·m^{-1} between the readout pulse and the compressed replica). Two optical circulators surround the fibre, enabling injection and extraction of counter-propagating light-waves at both ends. The input waveform to be compressed is injected from the right-hand side of the fibre. It is generated by means of a continuous-wave (CW) laser combined with an intensity modulator (IM) driven by a pulsed pattern generator (PPG) at a bit rate of 10 Mbit/s. The wavelength of this CW laser is adjusted to 1551 nm to perfectly match that of the readout pulse and guarantee phase-matching of the FWM interaction in the fibre [see Supplementary Information S1]. An Erbium-doped fibre amplifier (EDFA) and polarization controller (PC1) follow the modulator, respectively to amplify the input waveform to about 12-W peak power and to align its polarization state at 45° with respect to the *slow* and *fast* axes of the fibre, hence maximizing the FWM efficiency with balanced power in between the polarization components [see Methods].

From the opposite side, 6-ps readout pulses are injected at the same wavelength as the CW laser. They are generated by a 10-GHz actively mode-locked laser and are temporally gated through an intensity modulator, such that a single readout pulse can propagate within the fibre at any given time. Another EDFA boosts the peak power of these pulses to 3 W. A polarization controller (PC2) is then used to select the axis of the birefringent fibre (*fast* or *slow*) along which the readout pulse is injected, thereby enabling to choose if the compressed replica is time-reversed or not. At the output of the system, the residual readout pulse and the compressed waveform which have orthogonal polarizations, are separated with a polarizing beam splitter (PBS) before detection using unamplified 70-GHz photodetectors connected to a 63-GHz bandwidth real-time oscilloscope.

Temporal compression of optical data

Figure 2 shows typical experimental results based on an input waveform consisting of a 10-bit-long "1010011101" sequence cadenced at 10 Mbit/s (Fig. 2a, red). The input waveform extends over a 1-µs temporal window, corresponding to twice the fibre length. The blue curve in Fig. 2a (centred around zero for convenience) corresponds to a single-shot oscilloscope recording of the compressed replica measured in the counter-propagating direction when the polarization of the readout pulse is aligned along the *slow* axis of the birefringent fibre. When displayed on the same temporal scale as the input waveform, no details are discernible. An expanded view (Fig. 2b) clearly reveals that the counter-propagating signal carries the same binary sequence as the initial waveform but compressed onto an ultrafast 230-ps span. The observed timescale compression factor is M = 4,350, in excellent

agreement with the expected value of 4,378 (based on Eq. (1) and a group index n_g = 1.46). Overall, our system leads to an increase of the bit rate of the input sequence from 10 Mbit/s to 43.5 Gbit/s and a shortening of the individual bits from 50 ns to less than 13 ps. Note that the individual "1"s of the compressed sequence are here limited by the temporal resolution of our photodetector [see the Supplementary Information S2].

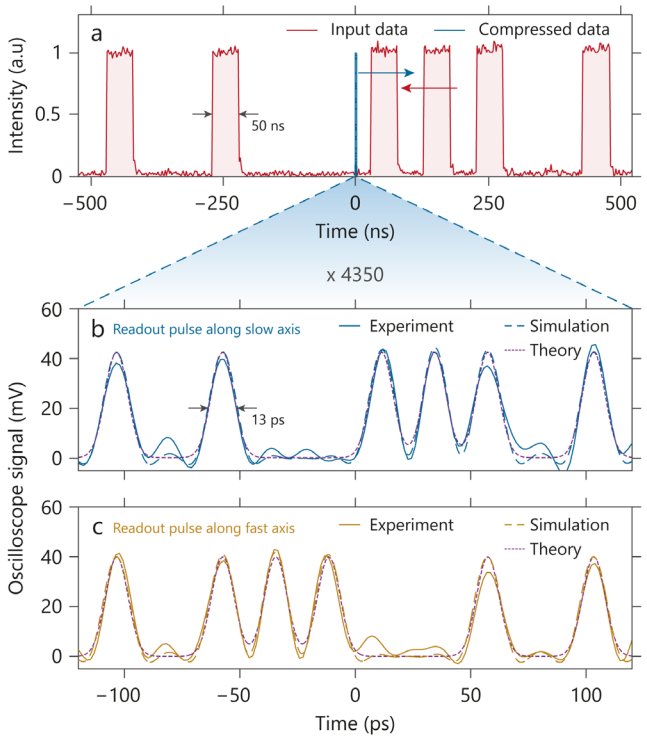

Figure 2 | Experimental demonstration of temporal compression of a 10-Mbit/s, 10-bit-long sequence into a 43.5-Gbit/s replica. (a) Input waveform (red solid line) and temporally compressed replica (in blue) visualised on the same temporal scale and normalized to unity. **(b)** Expanded view of the compressed waveform when the readout pulse propagates on the *slow* axis of the birefringent fibre, demonstrating an M = 4,350 timescale compression factor. **(c)** Same as in b, but with the readout pulse propagating along the *fast* axis, demonstrating time-reversal on top of temporal compression. Dashed lines in (b-c) are results from numerical simulations based on Eqs. (2), taking into account the bandwidth limitations of our detection apparatus. Purple dotted lines in (b-c) correspond to analytical predictions [see supplementary S2]. All amplitudes in (b&c) are normalized to experimental measurements, whilst temporal scales correspond to centred windows as they appear on the fast oscilloscope.

Our experimental results have been found to be in good agreement with numerical simulations (dashed line in Fig. 2b) based on a set of four coupled nonlinear Schrödinger equations for the two polarization components of each counter-propagating light-wave [see Eqs. (2) in Methods], as well as with the analytical predictions of ref. [39] (purple dotted line) [see Supplementary Information S2]. We have also performed measurements with a readout pulse propagating on the *fast* axis of the birefringent fibre. As reported in Fig. 2c, the compressed replica is then time-reversed. While expected from our description above, it is remarkable that a simple change of polarization state can lead to such a non-trivial functionality[5]. Again, simulation results (dashed line) and analytical predictions (dotted line) are in good agreement.

The results reported in Fig. 2 correspond to a record temporal compression ratio (4350 compared to the previous state-of-the-art of 27 in ref. [29]). In terms of absolute bit rates, our compressed signal (43.5 Gbit/s from a 10-Mbit/s initial data rate) does not surpass that reported in ref. [29] (270 Gbit/s from a 10-Gbit/s data sequence). We emphasize, however, this stems from our experiment using standard off-the-shelf components which prohibits single-shot detection of signals with faster bit rates: there is no fundamental limitation that would prevent our scheme to be applied on higher initial data rates to yield correspondingly faster compressed signals. We also note that the power efficiency of the compression process (defined as the ratio between the peak powers of the compressed signal and readout pulse) has been evaluated to be about 10^{-3} for the results shown in Fig. 2, leading to mW peak power at the system output [see Supplementary Information S3 for further discussions].

To assess the generality of this temporal compression process, we have performed additional experiments in three other fibres, with different levels of birefringence [see Table 1 in Methods for more details]. Each time, we experimentally deduced the compression factor M using an input waveform consisting of two 100-ns-long rectangular "bits" separated by 500 ns. Figure 3 summarizes the results of the whole measurements (black dots). This plot demonstrates that we can achieve compression factors up to about 13,000 with commercially available birefringent optical fibres, thus potentially enabling the generation of THz-bandwidth signals from ordinary MHz-systems. Furthermore, excellent agreement is obtained with the simple prediction of Eq. (1) (blue line) as well as with full numerical simulations [yellow triangles; based on Eqs. (2)]. This confirms the accuracy of Eq. (1) for design purpose.

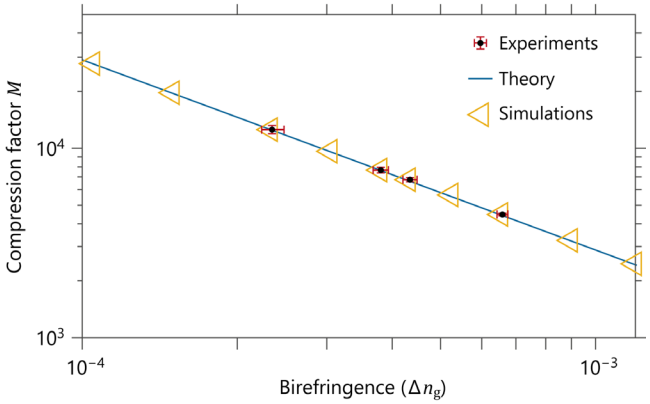

Figure 3 | Temporal compression factor M versus fibre birefringence. Black dots are experimental values measured in four different birefringent fibres using a two-bit input waveform (details in the text); red crosses indicate uncertainties (standard deviation). Blue line: prediction of Eq. (1). Yellow triangles: prediction based on numerical integration of Eqs. (2).

Temporal compression of arbitrary optical waveforms

The experiments reported above constitute a key proof-of-concept demonstration of the temporal focusing mirror compression scheme envisioned theoretically more than 25 years ago by Starodumov[39]. The results demonstrate several orders-of-magnitude compression of ON/OFF data, but the method has much further potential. In particular, beyond digital data sequences, the scheme can be applied to arbitrary optical waveforms, providing that the readout pulse duration and the walk-off rate are suitably selected. To illustrate this point, we performed additional experiments [see Methods] in which an electronic MHz-bandwidth arbitrary waveform generator was used to define a non-trivial optical waveform as the initial signal [red curve in Fig. 4a]. As in Fig. 2, the blue line in Fig. 4a shows the single-shot recording of the compressed waveform on the same temporal scale as the input waveform, while Fig. 4b provides an expanded view around the compressed replica. As can be seen, the compressed signal is a faithful replica of the input arbitrary waveform, though slight distortions can be observed due to the bandwidth limitations of our detection scheme, but temporally compressed by a factor of 4350.

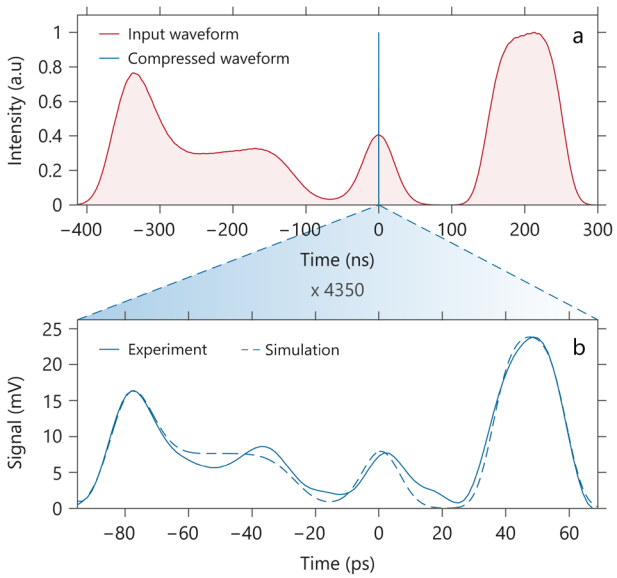

Figure 4 | Experimental result of temporal compression of a MHz-bandwidth arbitrary waveform into a multi-GHz replica. (a) Input waveform (red) and temporally compressed signal (blue) displayed on the same temporal scale. **(b)** Expanded view of the compressed waveform, demonstrating the generation of a 4,350-timescale compressed replica. Dashed lines in (b) are results from numerical simulations based on Eqs. (2). The amplitudes in (b) are normalized to experimental measurements.

To further demonstrate the potential of the compression scheme across scales and illustrate the limitation imposed by the readout pulse duration, Fig. 5 shows results of numerical simulations of a waveform portraying the elevation profile of the Te Paki coastal track located in the far north of New Zealand. The incident signal is shown at the top of Fig. 5 (red) and takes the form of a 1-µs-long non-trivial analog waveform. The simulated temporal compression takes place in a 100-m long fibre segment, with four different values of birefringence leading to compression factors ranging from 10^2 to $3{\cdot}10^4$. As these cover multiple orders of magnitude, we consider here a 1-ps duration readout pulse (shown in green at the bottom of Fig. 5) to guarantee a good temporal resolution across. Peak powers are similar to those in our experimental demonstrations. In all four cases, we can clearly observe (left side of Fig. 5) the successful generation of high fidelity compressed replicas (cross-correlation coefficient better than 95%), with a reduction of the temporal span of the overall waveform to less than 30 ps for the smallest birefringence considered. Note that for this last specific case, a slight distortion can be observed on the resulting compressed waveform due to the convolution between the initial signal and the temporal-response of the compressor $M\tau$. However, a better fidelity and even larger compression factors could be achieved using sub-ps readout pulses.

Also shown on the right side in Fig. 5 are the RF spectra corresponding to each of the compressed waveforms. These illustrate how the temporal focusing mirror can convert a MHz-bandwidth input signal into a THz-bandwidth output, thus highlighting the scheme's potential for ultra-fast arbitrary optical waveform generation. Furthermore, because of the phase-conjugation nature of the underlying FWM interaction, we note that the scheme could also be applied to compress phase-encoded data. Finally, we expect the compression factor to also scale the timing jitter. Starting with very low jitter electronic generators, this could enable the generation of THz-bandwidth signals with attosecond residual timing jitter. We note however before closing that, although the present method is able to increase the repetition rate of data packets and compress individual waveforms, increasing the global bit rate of a transmission line would necessitate the compression method to be combined with a time multiplexing scheme to temporally aggregate the successive ultra-fast data packets[39].

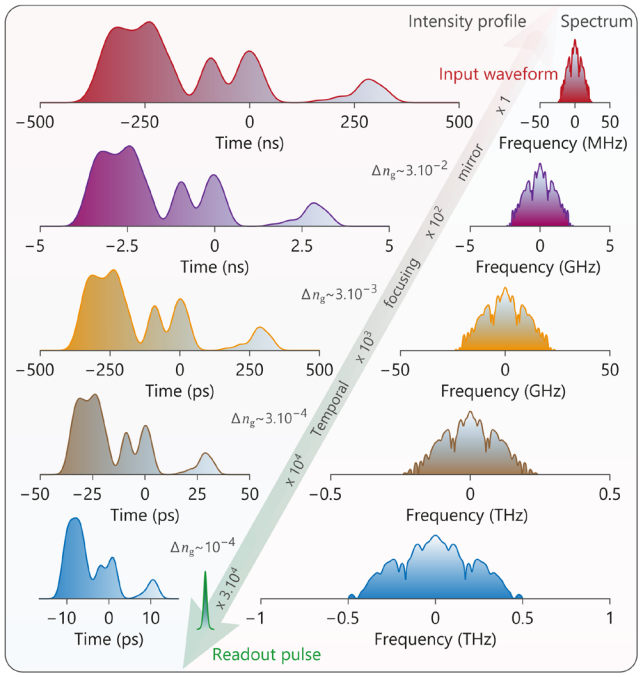

Figure 5 | Numerical results showing the temporal compression of an analog optical waveform for different values of fibre birefringence. The left and right areas of the figure depict, respectively, the output temporal intensity profiles normalized to unity and the corresponding RF spectra on a 30-dB vertical scale. The incident waveform is depicted at the top in red, whilst the counter-propagating 1-ps readout pulse is displayed in green at the bottom. Purple: $\Delta n_g = 3{\cdot}10^{-2}$, $M = 10^2$; ochre: $\Delta n_g = 3{\cdot}10^{-3}$, $M = 10^3$; brown: $\Delta n_g = 3{\cdot}10^{-4}$, $M = 10^4$; blue: $\Delta n_g = 10^{-4}$, $M = 3{\cdot}10^4$.

4. Discussion

To conclude, we have experimentally implemented a fully-degenerate variant of Starodumov's scheme[39] for the compression of optical pulse trains and demonstrated the real-time temporal compression of optical waveforms by factors ranging from 4,350 to 13,000. This represents two orders of magnitude improvement with respect to previously demonstrated temporal compression schemes based, e.g., on time lenses[28-29], whilst using a much simpler setup. In that regard, we must reiterate that the results demonstrated here are not constrained by any fundamental limits; rather we have selected our parameters to fall within the direct detection bandwidth of our 70-GHz photodetectors, while using standard off-the-shelf components. The level of birefringence ($<10^{-3}$) associated with commercially available polarization maintaining fibers limit the compression capabilities of the system to large compression factors (typically above M=3000). However, more recent microstructured optical fiber designs and engineered integrated waveguides can feature ultra-high levels of birefringence ($>10^{-3}$), which could be used to achieve substantially lower compression factors (100<M<3000)[44-47]. In this context, we envision that our implementation is fully scalable to different photonic platforms[47-49], including integrated photonics[47,49], which could offer scaling factors from 10^2 to 10^5 and support compression to Gbit/s or Tbit/s repetition-rates, from low-cost, low-bandwidth generators. From a more general perspective, beyond optical communications, this all-optical, conceptually simple, temporal compression system, could find numerous applications in many fields of science where cost-effective generation of ultrafast optical data, pulse trains, or waveforms is required.

References

1. Wong, T. *et al.* Asymmetric-detection time-stretch optical microscopy (ATOM) for ultrafast high-contrast cellular imaging in flow. *Sci. Rep.* **4**, 3656 (2014).
2. Roussel, E. *et al.* Observing microscopic structures of a relativistic object using a time-stretch strategy. *Sci Rep* **5**, 10330 (2015).
3. Herink, G., Kurtz, F., Jalali, B., Solli, D. R. & Ropers, C. Real-time spectral interferometry probes the internal dynamics of femtosecond soliton molecules. *Science* **356**, 50–54 (2017).
4. Lei, M., Zou, W., Li, X. & Chen, J. Ultrafast FBG interrogator based on time-stretch method. *IEEE Photon. Technol. Lett.* **28**, 778–781 (2016).
5. Palushani, E. *et al.* All-optical OFDM demultiplexing by spectral magnification and band-pass filtering. *Opt. Express* **22**, 136–144 (2014).
6. Bennett, C. V., Scott, R. P. & Kolner, B. H. Temporal magnification and reversal of 100 Gb/s optical data with an up-conversion time microscope. *Appl. Phys.Lett*. **65**, 2513–2515 (1994).
7. Foster, M. A. *et al.* Silicon-chip-based ultrafast optical oscilloscope. *Nature* **456**, 81–84 (2008).
8. Mahjoubfar, A. *et al.* Time stretch and its applications. *Nature Photon* **11**, 341–351 (2017).
9. Kolner, B. H. & Nazarathy, M. Temporal imaging with a time lens. *Opt. Lett.* **14**, 630–632 (1989).
10. Kolner, B. H. Space-time duality and the theory of temporal imaging. *IEEE J. Quantum Electron*. **30**, 1951–1963 (1994).
11. Azaña, J. Time-to-frequency conversion using a single time lens. *Optics Commun*. **217**, 205–209 (2003).
12. Salem, R., Foster, M. A. & Gaeta, A. L. Application of space–time duality to ultrahigh-speed optical signal processing. *Advances in Optics and Photonics* **5**, 274–317 (2013).
13. Goda, K., Jalali, B. Dispersive Fourier transformation for fast continuous single-shot measurements. *Nature Photon* **7**, 102–112 (2013).
14. Solli, D., Ropers, C., Koonath, P. & Jalali, B. Optical rogue waves. *Nature* **450**, 1054–1057 (2007).
15. Närhi, M. *et al.* Real-time measurements of spontaneous breathers and rogue wave events in optical fibre modulation instability. *Nat Commun* **7**, 13675 (2016).
16. Suret, P. *et al.* Single-shot observation of optical rogue waves in integrable turbulence using time microscopy. *Nat Commun* **7**, 13136 (2016).
17. Meng, F. *et al.* Intracavity incoherent supercontinuum dynamics and rogue waves in a broadband dissipative soliton laser. *Nat Commun* **12**, 5567 (2021).
18. Runge, A. F., Broderick, N. G. & Erkintalo, M. Observation of soliton explosions in a passively mode-locked fibre laser. *Optica* **2**, 36–39 (2015).
19. Herink, G., Jalali, B., Ropers, C. & Solli, D. Resolving the build-up of femtosecond mode-locking with single-shot spectroscopy at 90 MHz frame rate. *Nature Photon* **10**, 321–326 (2016).
20. Ryczkowski, P. *et al.* Real-time full-field characterization of transient dissipative soliton dynamics in a mode-locked laser. *Nature Photon* **12**, 221–227 (2018).
21. Asghari, M. H. & Jalali, B. Experimental demonstration of optical real-time data compression. *Appl. Phys. Lett.* **104**, 111101 (2014).
22. Jalali, B., Chan, J. & Asghari, M. H. Time-bandwidth engineering. *Optica* **1**, 23–31 (2014).
23. Rangarajan, S., Poulsen, H. N. & Blumenthal, D. J. All-Optical Packet Compression of Variable Length Packets From 40 to 1500 B Using a Gated Fibre Loop. *IEEE Photon. Technol. Lett*. **18**, 322–324 (2006).
24. Deng, K.-L., Kang, K. I., Glesk, I., Prucnal, P. R. & Shin, S. Optical packet compressor for ultra-fast packet-switched optical networks. *Electron. Lett.* **33**, 1237–1238 (1997).
25. Toda, H., Nakada, F., Suzuki, M. & Hasegawa, A. An optical packet compressor based on a fibre delay loop. *IEEE Photon. Technol. Lett.* **12**, 708–710 (2000).
26. Toliver, P., Deng, K.-L., Glesk, I. & Prucnal, P. R. Simultaneous optical compression and decompression of 100-Gb/s OTDM packets using a single bidirectional optical delay line lattice. *IEEE Photon. Technol. Lett*. **11**, 1183–1185 (1999).
27. Sotobayashi, H., Kitayama, K. & Ozeki, T. 40 Gbit/s photonic packet compression and decompression by supercontinuum generation. *Electron. Lett.* **37**, 110–111 (2001).
28. Almeida, P. J., Petropoulos, P., Thomsen, B. C., Ibsen, M. & Richardson, D. J. All-optical packet compression based on time-to-wavelength conversion. *IEEE Photon. Technol. Lett*. **16**, 1688–1690 (2004).
29. Foster, M. *et al.* Ultrafast waveform compression using a time-domain telescope. *Nature Photon.* **3**, 581–585 (2009).
30. Cundiff, S. & Weiner, A. Optical arbitrary waveform generation. *Nature Photon* **4**, 760–766 (2010).
31. Wang, J., Shen, H., Fan, L. *et al.* Reconfigurable radio-frequency arbitrary waveforms synthesized in a silicon photonic chip. *Nat Commun* **6**, 5957 (2015).
32. Rouskas, G. N. & Xu L. Optical packet switching. In: Sivalingam K.M., Subramaniam S. (eds) Emerging optical network technologies. Springer, Boston, MA (2005).
33. Yoshida Y. *et al.* SDN-based network orchestration of variable-capacity optical packet switching network over programmable flexi-grid elastic optical path network. *J. Lightwave Technol.* **33**, 609–617 (2015).
34. Wohlleben, W., Buckup, T., Herek, J. L. & Motzkus, M. Coherent control for spectroscopy and manipulation of biological dynamics. *ChemPhysChem.* **6**, 850–857 (2005).
35. Wu, H., Zhu, W., Pang, J. & Cheng, Z. Research on superconducting Qubit manipulation based on arbitrary waveform generator. *Journal of Physics*: Conference Series **1650**, (2020).
36. Ng, W., Rockwood, T., Sefler, G. & Valley, G. Demonstration of a large stretch-ratio (M=41) photonic analog-to-digital converter with 8 ENOB for an input signal bandwidth of 10 GHz. *IEEE Photon. Technol. Lett*. **24**, 1185–1187 (2012).
37. Goda, K., Tsia, K. K. & Jalali, B. Serial time-encoded amplified imaging for real-time observation of fast dynamic phenomena. *Nature* **458**, 1145–1149 (2009).
38. Khilo, A. *et al.* Photonic ADC: overcoming the bottleneck of electronic jitter. *Opt. Express* **20**, 4454–4469 (2012).
39. Starodumov, A. N. Pulse train compression up to terabit rates using four-wave mixing in birefringent fibre. *Optics Commun*. **124**, 365–372 (1996).
40. Kaplan, A. E. Optical bistability that is due to mutual self-action of counterpropagating beams of light. *Opt. Lett.* **6**, 360–362 (1981).
41. Guasoni, M. *et al.* Line of polarization attraction in highly birefringent optical fibres. *J. Opt. Soc. Am. B* **31**, 572–580 (2014).
42. Gauthier, D. J., Malcuit, M.S., Gaeta A. L. & Boyd R. W. Polarization bistability of counterpropagating laser beams. *Phys. Rev. Lett.* **64**, 1721 (1990).
43. Dawes, A. M. C., Illing, L., Clark, S. M. & Gauthier, D. J. All-Optical Switching in Rubidium Vapor. *Science* **308**, 672–674 (2005).
44. Beltrán-Mejía F. *et al.* Ultrahigh-birefringent squeezed lattice photonic crystal fiber with rotated elliptical air holes. *Opt. Lett.* **35**, 544–546 (2010).
45. Jung, Y., Brambilla, G., Oh, K. & Richardson, D. J. Highly birefringent silica microfiber. *Opt. Lett.* **35**, 378–380 (2010).
46. Yang T. *et al.* High birefringence photonic crystal fiber with high nonlinearity and low confinement loss. *Opt. Express* **23**, 8329–8337 (2015).
47. Zhou, J. *et al.* Electro-optically switchable optical true delay lines of meter-scale lengths fabricated on Lithium Niobate on insulator using photolithography assisted chemo-mechanical etching. *Chin. Phys. Lett*. **37**, 084201 (2020).
48. Zhang, H., Bigot-Astruc, M., Bigot, L., Sillard, P. & Fatome, J. Multiple modal and wavelength conversion process of a 10-Gbit/s signal in a 6-LP-mode fibre. *Opt. Express* **27**, 15413–15425 (2019).
49. Li, B. *et al.* Reaching fiber-laser coherence in integrated photonics. *Opt. Lett*. **46**, 5201–5204 (2021).
50. Agrawal, G. P. *Nonlinear Fibre Optics*. 5th ed., Academic Press, Oxford, (2013).

Methods

Experimental setup. In our experiments, the initial waveform to be compressed is generated from a continuous-wave (CW) laser centred at λ=1551 nm that is modulated in the temporal domain by means of a Mach-Zehnder electro-optic intensity modulator (IM). For the temporal compression of the 10-Mbit/s sequence reported in Fig. 2, the IM is driven by a 10-Gbit/s pulse pattern generator (PPG) that is synchronized to a 10-GHz common RF clock. A 10-Gbit/s 100,000-bit-length sequence is programmed on the PPG to generate an optical 10-bit return-to-zero data packet "1010011101" cadenced at 10 Mbit/s with 50 ns pulse duration, representing twice the fibre length used for the results presented in Fig. 2. Because of the long 50-ns individual bit duration, the data packet is further phase modulated (PM) with a 73-MHz RF tone so as to limit the stimulated Brillouin backscattering (SBS) in the fibre

under test. (It is worth noting that such phase modulation would not be required for input data rates faster than 1 Gbit/s, as in this case the signal would have sufficient bandwidth to be effectively immune to SBS.) Regarding the temporal compression of arbitrary waveform reported in Fig. 4, the IM is driven by a standard MHz-bandwidth arbitrary waveform generator from Keysight (81150A), triggered by the 10-Gbit/s PPG described above for synchronization purpose. The waveform involved in Fig. 4 consists in an arbitrary shape made of 32768 samples. The initial waveforms are then amplified by means of an Erbium doped fibre amplifier (EDFA) from Lumibird to yield an average power of 0.4 W, corresponding to a pulse peak power of 12 W for the data sequence shown in Fig. 2. Before the signal is launched into the fibre under test, a polarization controller (PC1 in Fig. 1) is used to align the polarization of the signal at 45° of the fibre's birefringent axes. Note that this polarization alignment is not particularly critical but confers maximal energy to the compressed replica.

At the opposite end of the system, the counter-propagating readout pulses are generated from a 10-GHz picosecond laser synchronized to the same common 10-GHz RF clock than the PPG used to generate the data sequence to be compressed. The repetition-rate of the pulse train is decreased down to 2 MHz using a second intensity modulator driven by the same PPG. This repetition-rate reduction allows us to ensure that a single readout pulse is injected into the fibre at any given time, thus facilitating the data recording and interpretation of the results. The readout pulses are amplified using a second EDFA to reach a pulse peak power of 3 W at the fibre input. A 1-nm gaussian bandpass filter is also used to suppress excess noise and limit the spectral expansion of the readout pulse at the EDFA output. Finally, an inline polarizer was added to improve the polarization extinction ratio of the readout pulses to above 20 dB. A second-harmonic autocorrelator was used to measure the readout pulse duration at the input of the birefringent fibre, yielding a result of 6 ps (full-width at half-maximum). The readout pulses are subsequently injected into the birefringent fibre along one of the fibre's principal axes by means of a second polarization controller (PC2) spliced directly onto an optical circulator. Depending on the chosen axis, one can select the sign of the birefringence-induced group-delay between the readout pulse and the compressed replica, which determines whether the compressed waveform is time-reversed or not. Note that the polarization alignment of the readout pulse was finely controlled and adjusted by suppressing any residual orthogonal delayed components at the output of the fibre in absence of the counter-propagating waveform.

The fibre used in the temporal compression results shown in Fig. 2 consists of a 103-m long segment of polarization maintaining fibre from iXblue photonics characterized by a birefringence of $\Delta n_g = 6.67 \times 10^{-4}$ resulting in a temporal walk-off of 2.22 ps·m^{-1}. The fibre exhibits an anomalous second-order group-velocity dispersion coefficient D = 8.9 ps·nm^{-1}.km^{-1} at the signal wavelength and a nonlinear Kerr coefficient γ = 3 W^{-1}·km^{-1}. The fibre losses are below 1 dB·km^{-1}. Note that, to allow higher levels of injected powers and thus achieve a better efficiency, the fibre or the waveguide under test could be designed to operate in the normal dispersion regime at the signal wavelength, thus avoiding modulation instabilities of the long incident waveform, as well as soliton pulse-compression dynamics of the readout pulse [See Supplementary Information S4 for further details regarding the system limitations.] Finally, at the output of the system, a third polarization controller PC3, combined with a polarizing beam splitter (PBS) is used to separate the temporally compressed waveform and the residual readout pulse before temporal characterization by means of 70-GHz unamplified photodetectors from Finisar (XPDV3120R), with a measured responsivity of 0.4 A/W and connected to a 63-GHz real-time oscilloscope from Keysight (Infiniium DSO-X-93304Q featuring 160 GS/s), triggered by the initial 10-Mbit/s sequence. Note that the detection optical path features 3.1 dB of losses beyond the compression fibre.

Fibre parameters. The parameters of the optical fibres used in the experiments reported in Fig. 3 to measure the temporal compression factors *M* as a function of birefringence are summarized in Table 1. The birefringence was estimated by first measuring the length of the fibre segment using a commercial optical time domain reflectometer (OTDR), and then evaluating the birefringence-induced group-delay by injecting the readout pulse at 45° of the principal axes.

Provider	Length m	Birefringence Δn_g	Losses dB·km^{-1}	D ps·nm^{-1}·km^{-1}	γ W^{-1}·km^{-1}
iXblue	103	6.67 10^{-4}	0.7	8.9	3
iXblue	110	4.3 10^{-4}	0.4	1.5	2.5
iXblue	208	3.8 10^{-4}	0.6	7.3	2
ofs	510	2.3 10^{-4}	0.8	–1.3	8.4

Table 1 | Fibre parameters used for the experimental results of Fig. 3.

Modelling: coupled nonlinear Schrödinger equations. The interaction between two counter-propagating waves that propagate at the same frequency ω in a birefringent waveguide with cubic nonlinearity can be described in terms of the following set of coupled nonlinear Schrödinger equations[41,50]:

$$\begin{cases} \left(\partial_t + v_{g_x}\partial_z + i\frac{\beta_2}{2}\partial_{tt}\right)E_x = i\gamma\left[|E_x|^2 + \frac{2}{3}|E_y|^2 + 2|\overline{E_x}|^2 + \frac{2}{3}|\overline{E_y}|^2\right]E_x + i\frac{2\gamma}{3}E_y\overline{E_yE_x^*} \\ \left(\partial_t + v_{g_y}\partial_z + i\frac{\beta_2}{2}\partial_{tt}\right)E_y = i\gamma\left[|E_y|^2 + \frac{2}{3}|E_x|^2 + 2|\overline{E_y}|^2 + \frac{2}{3}|\overline{E_x}|^2\right]E_y + i\frac{2\gamma}{3}E_x\overline{E_xE_y^*} \\ \left(\partial_t - v_{g_x}\partial_z + i\frac{\beta_2}{2}\partial_{tt}\right)\overline{E_x} = i\gamma\left[|\overline{E_x}|^2 + \frac{2}{3}|\overline{E_y}|^2 + 2|E_x|^2 + \frac{2}{3}|E_y|^2\right]\overline{E_x} + i\frac{2\gamma}{3}\overline{E_y}E_yE_x^* \\ \left(\partial_t - v_{g_y}\partial_z + i\frac{\beta_2}{2}\partial_{tt}\right)\overline{E_y} = i\gamma\left[|\overline{E_y}|^2 + \frac{2}{3}|\overline{E_x}|^2 + 2|E_y|^2 + \frac{2}{3}|E_x|^2\right]\overline{E_y} + i\frac{2\gamma}{3}\overline{E_x}E_xE_y^* \end{cases} . \quad (2)$$

Here the optical fields $(E_x; E_y)$ describe the polarization components of the forward incident waveform propagating along the *slow (x)* and *fast (y)* axes of the birefringent fibre, whilst $(\overline{E_x}; \overline{E_y})$ describe the backward-propagating signal that consist of both the readout pulse and the compressed replica waveform. The variable *z* denotes the spatial coordinate along the fibre length, γ is the nonlinear Kerr coefficient and $v_{g_{(i)}}$ are the group-velocities of the waves along the *slow* (*x*) and *fast* axis (*y*) of the birefringent fibre under test. The first terms on the right-hand side of Eqs. (2) describe the action of self-phase modulation, the second, third, and fourth terms represent cross-phase modulation between co- and counter-propagating beams, and the last term represents the degenerate FWM interaction responsible for the energy flow between the two polarization components in each of the beams. Note that this energy exchange, reminiscent of phase-conjugated FWM interactions, is at the origin of the temporal compression mechanism, and it only occurs when both the forward and backward waves are present in the fibre and when the incident waveform is projected along both birefringent axes (45° maximizing the efficiency of the process). We must also point out that chromatic dispersion $\beta_2 = -\lambda^2 D/2\pi c$ has negligible impact in our experiments, as the characteristic dispersive lengths associated with the signal and readout pulses are at least one order of magnitude longer than the fibre length involved in the experiments[50] [See Supplementary Information S4 for further discussions.] For all the numerical simulations presented in this manuscript, a fourth-order Runge-Kutta integration scheme was used to integrate the nonlinear terms of the coupled equations presented in Eqs. (2).

Acknowledgements. We acknowledge A. Picozzi, P. Béjot, M. Guasoni, B. Kibler, C. Finot, A. Parriaux, G. Millot, H. Zhang, F. Leo, and Doc. S. Pitois for fruitful discussions. We also acknowledge T. Villedieu from iXblue for providing fibre parameters. JF acknowledges the financial support from the CNRS, IRP Wall-IN project (CNRS research collaboration agreement n°241655) and the financial support from the Conseil Régional de Bourgogne Franche-Comté, International Mobility Program. This work is supported by la délégation régionale à la recherche et à la technologie and the European Union through the PO FEDER-FSE Bourgogne 2014/2020 programs. This work has benefited from the facilities of the SMARTLIGHT platform in Bourgogne Franche-Comté (EQUIPEX+ ANR-21-ESRE-0040). SC and ME acknowledge the financial support from The Royal Society of New Zealand, in the form of Marsden Funding (18-UOA-310) and Rutherford Discovery Fellowships.